A Physical Simulation Model for Field Emission Triode

Chih-Wen Lu and Chung Len Lee, *Senior Member, IEEE*

***Abstract*— A simple but accurate physical model, which can be incorporated into circuit simulation programs such as SPICE for the *field emission triode* (FET), is developed. The model is based on the Fowler–Nordheim (F–N) current density–electric field (J–E) relationship. An electric field form is adopted to calculate the current density distribution along the surface of the sphere-shape tip. The cathode current is obtained by integration of the current density over the emission surface. The gate current is derived by the same integration, but over part of the emission area. A procedure to extract the values for the parameters of the model is also given. The model and the procedure has been applied to experimental devices to demonstrate its accuracy.**

***Index Terms*—Field emission triode, Fowler–Nordheim, simulation model.**

I. Introduction

FIELD emission triode (FET) is a solid-state device which features a miniature vacuum tube triode formed by application of modern intregrated circuit (IC) processing technology. It can be used in the applications such as flat panel display [1]–[4], microwave tubes [5]–[7]. A typical Spindt type FET consists of a cathode, a control gate, and an anode similar to that of a conventional vacuum tube triode. When a high voltage is applied between the gate and the cathode, a very large electric field is formed on the tip of the cathode due to the sharp geometry of the tip and the short gate-to-cathode distance. Following the Fowler–Nordheim (F–N) tunneling mechanism electrons will be emitted from the surface of the cathode to the anode which is biased at a proper high voltage [8]–[10]. However, since the gate is always biased more positively than the cathode, a large gate current can flow at the zero or moderate positive anode voltage.

The applications of FET in circuits have triggered a demand for its device model for circuit simulation. A simple, efficient and accurate FET model is pursued. Some works had been done on modeling the field emission diode [12]–[14] based on the F–N J-E relationship. In their approach, so-called electric field enhancement a and area b factors were used to transform the local J-E relationship to the global I–V characteristics. The approach is somehow questionable since the electric field is not constant across the tip and the factor b is a voltage dependent parameter [15]–[17]. A different approach, in which I–V equation is obtained through integration of the current density over the tip surface, is proposed by Nicolaescu and Avramescu [15]. In addition, Busta *et al.* [18] developed a model based on a numerical approach, from which the result obtained can serve as a guide for a more stringent theory. Jones *et al.* [19] also developed a circuit model for the FET array operating at the low-voltage. Qin *et al.* [20] also developed a model for the FET amplifier. Most recently, Lu *et al.* [21] developed an FET triode model with a parameter extraction procedure for SPICE simulation.

In this work, a new FET model which is based on the F–N tunneling mechanism, (but its J-E relationship is related with the device geometry parameters), is proposed. An extraction procedure is also derived to extract parameter values based on the device I–V characteristics. The model is developed on the diode as well as on the triode. Although the model is related with the device physical geometry parameters, the model is simple and easy to be incorporated into the circuit simulation program such as SPICE.

Manuscript received Jaunuary 5, 1998; revised April 13, 1998. The review of this paper was arranged by Editor C.-Y. Lu.

The authors are with the Department of Electronics Engineering, National Chiao Tung University, Hsinchu, Taiwan, R.O.C.

Publisher Item Identifier S 0018-9383(98)07451-6.

II. Device Model

The device model is first derived for a diode and then extended for a triode.

A. The Diode Model

Field emission diode modeling is generally based on the F–N J-E relationship which relates the field emission current density, J, to the electric field on the surface of the tip, E, and the work function, Φ. This relationship is given below as [9], [10]

$$J = AE^2 \exp\left(-\frac{B}{E}\right) \tag{1}$$

where

$$\begin{aligned} A &= \frac{1.55 \times 10^{-6}}{\Phi \cdot t^2(y)} \\ B &= 6.86 \times 10^7 \Phi^{3/2} v(y) \\ v(y) &= 0.95 - y^2 \\ y &= 3.79 \times 10^{-4} E^{1/2}/\Phi \\ t^2(y) &= 1.1 \end{aligned}$$

where J is expressed in terms of A/cm^2, E in volts/cm, and Φ in electron volts. In this approach, instead of lumping the total device current as a global parameter by treating J to be a constant over an effective area of the emission tip of the diode, we calculate the device current by integrating the current density by taking the variation of the electric field

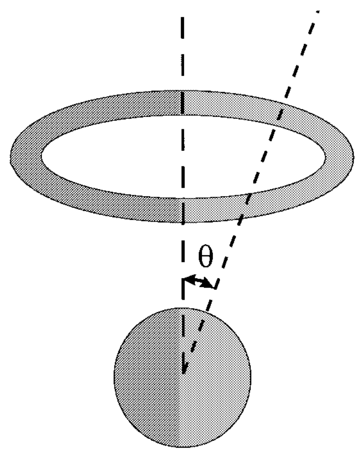

Fig. 1. The "Saturn" model, given by Jensen *et al.*, in which the tip is a floating sphere suspended near a ring of charge along the symmetry axis.

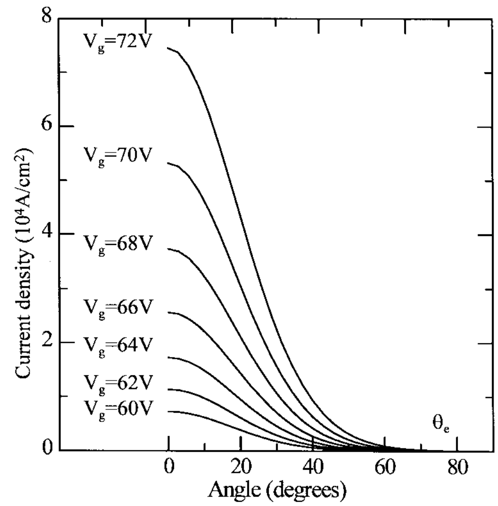

Fig. 2. The angular current density distribution calculated from (1)–(3) for several gate voltages. θ_e is the critical emission angle beyond which the emission becomes negligible. The larger the V_g, the larger the θ_e.

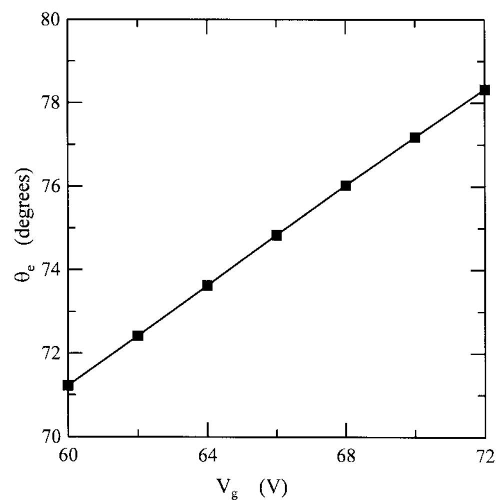

Fig. 3. The computed value of θ_e in terms of V_g from (1)–(3). The θ_e is defined as $J(\theta = \theta_e) = 0.1\% J(\theta = 0)$. The value of θ_e is almost linearly proportional to V_g.

across the surface of the tip into account. Hence, the electric field of the emission is first considered.

Previously, some work had been done on investigating the electric field of the emission tip of different shapes [22]–[24]. For example, Veen *et al.* investigated the electric field distribution of a tip of a shape of a paraboloid [23]. Jensen *et al.* [24] gave an expression for the electric field of a Saturn model which is shown in Fig. 1, where the tip is a floating sphere suspended at the symmetry axis of a gate of a ring shape. The field at the position which is at an angle of with respect to the symmetry axis of the surface is given by

$$E(\theta) = E_0/[1 + \lambda(1 - \cos(\theta))] \tag{2}$$

where E_0 is the maximum electric field at the position of $\theta = 0°$ of the sphere and λ is a fitting parameter. In this work, the Jenson's result is used for our approach where λ is taken 0.76. In fact, the electric field obtained by assuming $\lambda = 0.76$ is almost the same as that obtained from the Veen's model. The maximum difference between two field distributions is less than 1.5% for $\theta \leq 90°$. So, we consider that (2) is a good approximated formula for describing the electric field distribution on the surface near the apex of the tip. Hence, in this work, we assume that the shape of the tip near the apex is a sphere and its field distribution is that of (2).

In practice, the field emission current is measured as a function of the applied voltage. The conventional geometrical factor β is used to correlate the electric field at the apex of the tip to the voltage [25], i.e.,

$$E_0 = \beta V_g \tag{3}$$

With (1)–(3), the angular current density distribution can then be calculated. Fig. 2 shows a calculated angular current density distribution for several gate voltages for $\phi = 4.5$ eV and $\beta = 9.25 \times 10^5$ cm^{-1}, which is a value calculated by using the parameter extraction procedure which is to be presented later in this paper for the first demonstrated device. It can be seen that the current density is an exponential-like function of θ. The cathode current can then be obtained by integrating the current density over the emission surface of the tip, i.e.,

$$I_c = 2\pi r^2 \int_0^{\theta_e} J \sin\theta \, d\theta \tag{4}$$

where r is the radius of the sphere-shape tip and θ_e is the critical emission angle beyond which the current emission becomes negligible, i.e.,

$$J(\theta) = 0 \quad \text{for } \theta \geq \theta_e. \tag{5}$$

From Fig. 2, the value of θ_e is seen to be a function of V_g. The larger the gate voltage, the larger value of θ_e. This indicates that a larger V_g results in a larger emitting area. θ_e in terms of V_g can be computed from (1)–(3). Fig. 3 shows such a plot for the above example where θ_e is defined as $J(\theta = \theta_e) = 0.1\% J(\theta = 0)$. It can be seen that the value of θ_e is almost linearly proportional to the gate voltage.

Here, we also assume that the radius r of the tip is large enough to allow the planar F–N J-E relationship to be applied

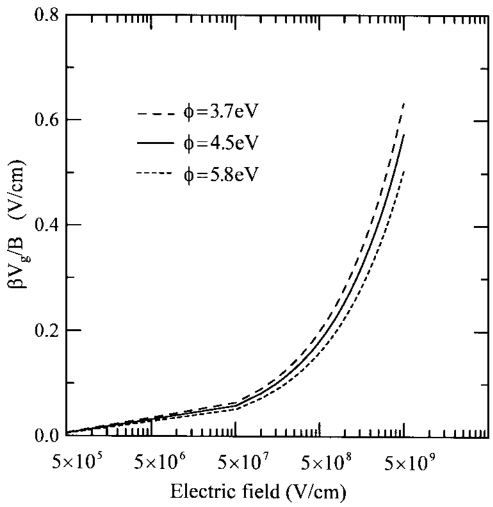

Fig. 4. The value of the term, $\beta V_g/B$, computed for several work functions. The value of this term is smaller than one even the electrical field is up to 5×10^9 V/cm.

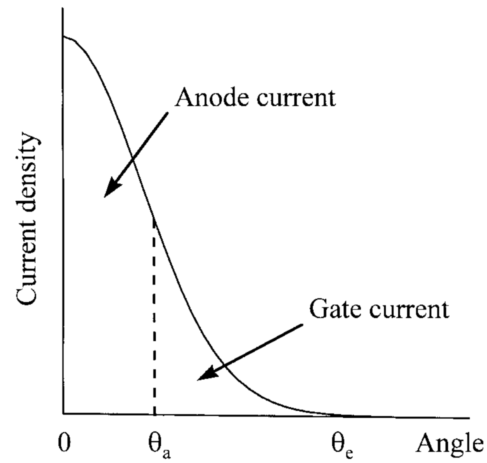

Fig. 5. The anode current component and the gate current component obtained from the current density distribution along the cathode surface respectively. θ_a is the angle beyond which the cathode emitted charges are collected by the gate to be the gate current. The anode collects emitted currents emitted from the cathode for the angles from $\theta = 0$ to θ_a.

[26] and the value of B in (1) is independent of electric field. Using (1)–(4), we can obtain the effective cathode current for an array of emission tips to be

$$I_c = -\frac{2\pi r^2 NA}{\lambda B}\beta^3 V_g^3 \frac{e^{(B\beta V_g)x}}{x^2}\sum_{n=0}^{\infty}(-1)^n(n+1)! \cdot \left(\frac{\beta V_g}{Bx}\right)^n \Big|_{\theta=0}^{\theta=\theta_c} \tag{6}$$

where $x = 1 + \lambda(1 - \cos\theta)$ and N is the number of the emission tips.

In (6), since $J(\theta = \theta_e) = 0$ from (5), the obtained cathode current is:

$$I_c = \frac{2\pi r^2 NA}{\lambda B}\beta^3 V_g^3 e^{-(B/\beta V_g)}\sum_{n=0}^{\infty}(-1)^n(n+1)!\left(\frac{\beta V_g}{B}\right)^n. \tag{7}$$

In (7), the term, $\beta V_g/B$, is a function of E_g. This term can be calculated by using (1) and (3). Fig. 4 plots the value of this term for several work functions. From this plot, it is seen that it is smaller than one even for the electric field up to 5×10^9 V/cm. The maximum electric field value in practice must be determined by the dielectric strength of the insulating material between the gate electrode and the substrate. Since the insulator is most likely to be silicon oxide or silicon nitride, the dielectric strength is lower than 5×10^8 V/cm. Hence, (7) converges. Also, in (7), it is noted that I_c is expressed in terms of the radius "r" of the emission tip and it is proportional to V_g^3, instead of V_g^2 as in the conventional field emission diode current-voltage expressions [9], [25].

B. The Triode Model

For a triode, the current emitted from the cathode is shared, mostly by the anode and by the gate. In this case, as in Fig. 5 which is the plot of one of curves of Fig. 2, the current emitted from within the surface of the tip from $\theta = 0$ to the angle θ_a is collected by the anode to be the anode current and the current emitted from the surface for the angle $\theta > \theta_a$ is collected by the gate to be the gate current. The gate current I_g can be obtained by integrating the emitted current density over the range of $\theta = \theta_a$ to $\theta = \theta_e$ from (1)–(3), i.e.,

$$\begin{aligned} I_g &= 2\pi r^2 N \int_{\theta_a}^{\theta_e} J \sin\theta \, d\theta \\ &= \frac{2\pi r^2 NA}{\lambda B}\beta^3 V_g^3 \frac{e^{(-B/\beta V_g)x_a}}{x_a^2}\sum_{n=0}^{\infty}(-1)^n(n+1)! \\ &\quad \cdot \left(\frac{\beta V_g}{Bx_a}\right)^n \end{aligned} \tag{8}$$

where

$$x_a = 1 + \lambda(1 - \cos\theta_a).$$

In (8), also $J(\theta = \theta_e) = 0$ from (5), hence I_g is a function of θ_a.

θ_a is a parameter related with the collecting ability of the anode. For a large anode voltage V_a, it gives a large value of θ_a. For the saturation region of the FET device, θ_a equals to θ_e and all the cathode emission current becomes the anode current. For the triode region, θ_a is between 0 and θ_e. Fig. 6 is the plots of the gate current I_g versus θ_a computed from (8) for a set of different gate voltages. These plots are very similar to those measured curves of the gate currents versus the anode voltage V_a. Hence, it is assumed that, for the triode region of the FET, θ_a is linearly proportional to V_a, i.e.,

$$\theta_a = \alpha(V_a - V_{aT}) \tag{9}$$

where V_{aT} is the threshold voltage of the FET device, above which the anode starts to collect the emitted currents. The value of V_{aT} is dependent on the anode configuration. A smaller distance from anode to gate gives a lower V_{aT}. V_{aT} is also dependent on the gate voltage. A larger gate voltage causes a larger value of V_{aT}.

To verify the above assumption, the values of θ_a versus V_a are computed from the data of Fig. 6 and the measured

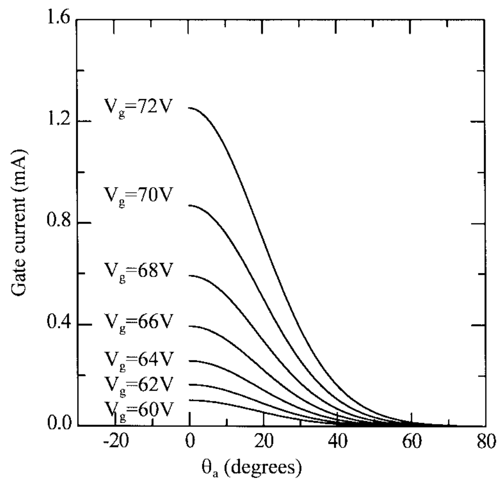

Fig. 6. The computed gate current as a function of the emission angle θ_a from (8) for different gate voltages.

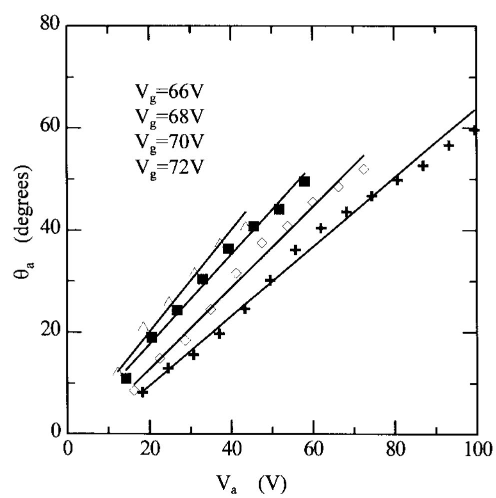

Fig. 7. The plots of the computed values of θ_a versus V_a which are computed from the data of Fig. 6 and the measured gate currents based on (8) for several gate voltages. Four plotted curves are roughly linear and their extrapolated points intersect at the horizontal axis at $V_a \cong 0$, 4, and 6 V for $V_g \leq 68$ V, $= 70$ V and $= 72$ V, respectively.

gate currents respectively for several gate voltages by using (8), and the results are plotted in Fig. 7. The plotted curves are approximately linear and their extrapolated values at the horizontal axis are approximately 0, 4, and 6 V for $V_g \leq 68$ V, $= 70$ V and $= 72$ V, respectively.

In the above equation, α is a factor which relates the anode voltage to the angle θ_a. It is expected to be a function of the gate voltage. Fig. 8 is the plots of θ_a versus V_g also computed by using (8) from the same Fig. 6 and the measured gate currents but with V_a as the varying parameters. It is seen that θ_a increases first, due to the increasing value of θ_e (see Fig. 3), with respect to V_g, then decreases due to the increasing emitting area collected by the gate (see Fig. 4). Hence it is then assumed that α is a function of V_g of second order polynomials, i.e.,

$$\alpha = a_0 + a_1 V_g + a_2 V_g^2 \tag{10}$$

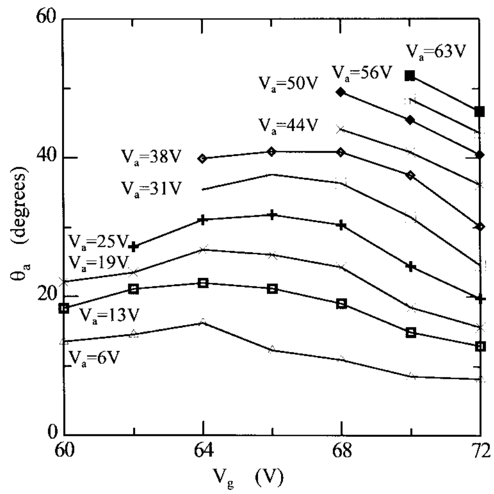

Fig. 8. The plots of θ_a versus V_g computed by using (8) from Fig. 6 and the measured gate currents but with V_a as the varying parameters. θ_a increases first then decreases with respect to V_g for all V_a.

where a_0, a_1, and a_2 are parameters to be extracted in the later extraction procedure.

Since the emission current always equals the anode current plus the gate current, the anode current I_a can be obtained by subtracting the gate current I_g of (8) from the cathode current I_c of (7), i.e.,

$$I_a = I_c - I_g. \tag{11}$$

III. Parameter Extraction Procedure

In this section the extraction procedure for values of the necessary parameters of the above (7)–(10) are described. To describe the procedure more clearly, device data which were published in this area are used as demonstration examples.

The first device example used is that published in the Betsui's paper [11]. The device was an silicon field emitter arrays of 6400 (80 $\times$ 80) tips. The radius of the bullet-shaped tip was reported being less than 20 nm. The spacing between tips was 4μm, so the tip density was 6.25 $\times$ 10^6 cm^{-}2. The diameter of the gate aperture was 2μm, which was larger than that of its silicon dioxide mask. The distance between the anode plate and gate was 1 mm. In Betsui's measuring apparatus, the gate was grounded and negative voltage was applied to the cathode to extract electrons. In this work, the cathode voltage is assumed to be the reference grounded voltage.

In (7)–(10), $\phi, r, N, \lambda, \beta, \alpha$, and V_{aT} are unknown parameters. In the extraction procedure, these parameters are not extracted individually. They are extracted through two parameters: A' and B'. A' is a parameter related with the emission area and B' is a parameter related with the geometrical factor β:

$$A' = \frac{2\pi r^2 NA}{\lambda B}\beta^3 \sum_{n=0}^{\infty}(-1)^n(n+1)!\left(\frac{\beta V_g}{B}\right)^n \tag{12a}$$

and

$$B' = \frac{B}{\beta}. \tag{12b}$$

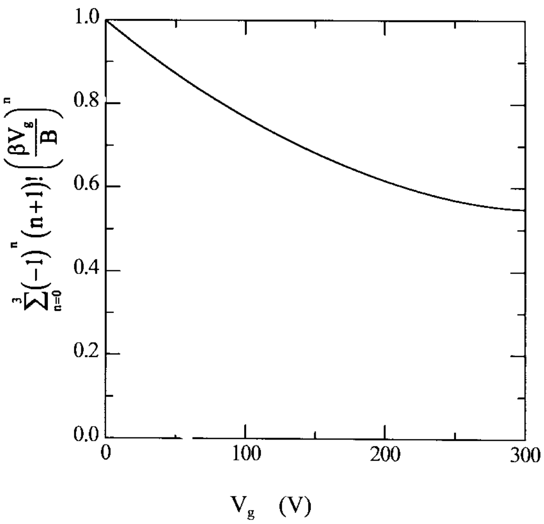

Fig. 9. The computed summation of the first four terms of the summation part, $\Sigma_{n=0}^{3}(-1)^n(n+1)!(\beta V_g/B)^n$, of the parameter A' as a function of V_g for $\beta = 9.25 \times 10^5$ cm^{-1} and $\phi = 4.5$ eV. It is a slowly varying function of V_g for the whole 0–300 V gate voltage region.

With these two parameters, the emission current can be expressed as:

$$I_c = A' V_g^3 e^{-(B'/V_g)}. \tag{13}$$

Fig. 9 plots the value of the summation of the first four terms of the summation part of the parameter A' versus V_g for taking $\beta = 9.25 \times 10^5$ cm^{-1} and $\phi = 4.5$ eV (It is of enough accuracy by just taking the first four terms since the term $[\beta V_g/B]^n$ converges fast). It can be seen that for the whole 0–300 V gate voltage region it is a slowly varying function of V_g. Hence, it can be considered to be constant during extraction. Also, it was reported that the parameter B is a slowly varying function of V_g [27], hence the parameter B' is also a slowly varying function of V_g. It can also be considered to be constant during extraction.

Since we can rearrange (13) as

$$\ln \frac{I_c}{V_g^3} = \ln\ A' - \frac{B'}{V_g} \tag{14}$$

for the diode characteristics, we can plot $\ln(I_c/V_g^3)$ versus $1/V_g$ to obtain a straight line. From the slope and the intersection of the straight line with the coordinate axis, the values of A' and B' can be obtained. Fig. 10 shows such a plot of the device, which were operated at $V_a = 260$ V. The plotted curve is seen to be a straight line. The values obtained for A' and B' are 6.27 $\times$ 10^{-5} A/V^3 and 708 V, respectively. The term of $(2\pi r^2 NA/\lambda B)\beta^3$, which is a slowly varying function of V_g, in the gate current equation, can be obtained from the values of A' and B' from (12a) and (12b), respectively. For this example, its value is 6.22 $\times$ 10^{-5}+ 1.94 $\times$ $10^{-7} V_g$. The values of A', B', and $(2\pi r^2 NA/\lambda B)\beta^3$ of this example are compiled in Table I. From these values, if the work function Φ and the number of tips are known, the radius r of the tip can be estimated. For this example, the number of tips is 6400. A value of 19 nm is obtained for the radius r of the tip if a work function of 4.5 eV and $v(y) = 1$ is assumed. This value is consistent with that reported in [11].

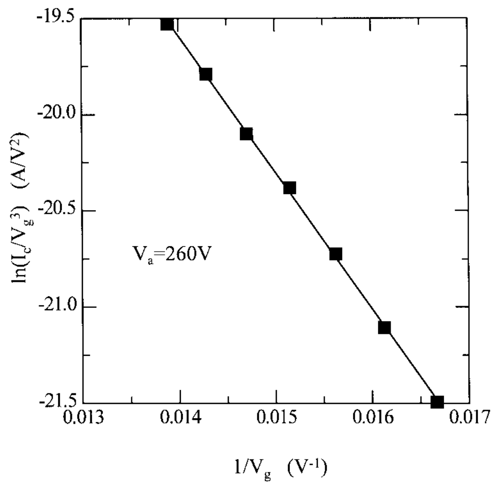

Fig. 10. The $\ln(I_c/V_g^3)$ versus $1/V_g$ plot of the cathode current of the experimental device operating at $V_a = 260$ V. It is a closely approximated straight line as $\ln(I_c/V_g^3) = \ln(6.27 \times 10^{-5}) - (708/V_g)$.

TABLE I
EXTRACTED PARAMETERS OF THE FIRST EXAMPLE

Parameter or Term	Value or Function
A'	6.27×10^{-5} A/V^3
B'	708 V
$\dfrac{2\pi r^2 NA}{\lambda B}\beta^3$	$6.22 \times 10^{-5} + 1.94 \times 10^{-7} V_g$ A/V^3
V_{aT}	**0V ($V_g \le 68$V)**
	4V ($V_g = 70$V)
	6V ($V_g = 72$V)
a_0	-8.77×10^{-1} **degrees/volts**
a_1	1×10^{-1} **degrees/volts**
a_2	-1.1×10^{-3} **degrees/volts**
r	19nm

To this point, the only two parameters of unknown values are α and V_{aT}. Their values can be obtained from Fig. 7. In the figure, the slope and the intersection of straight lines with the V_a coordinate axis for each V_g, give the values of α and V_{aT}. For this example, V_{aT} is determined to be approximately 0, 4, and 6 V for $V_g \le 68$ V, $= 70$ V and $= 72$ V, respectively, and the values of determined as a function of V_g are plotted in Fig. 11, where the square dots are the extracted data and the solid line is the fitted curve for (10). The fitted values for parameters a_0, a_1, and a_2 are also shown in Table I.

With all the values obtained in Table I, the gate current can be calculated and reconstructed from (8) and (9). Fig. 12 shows the reconstructed gate current (the solid curves) versus V_a with the measured data (the dotted curves). With the cathode and gate currents obtained, the anode current is calculated from (11) and is shown in Fig. 13. In the above two figures, the calculated reconstructed currents and the measured currents match very well.

To verify the accuracy of this model, a second example is also given. Fig. 14 shows the I–V characteristics of an FET triode with 100 emitter tips [28], where the dotted curves are

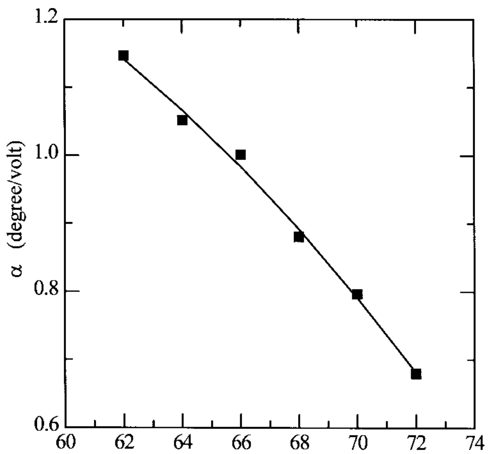

Fig. 11. The extracted α as a function of V_g for the experimental device of [11]. The square dots are the extracted data and the solid line is the fitted curve for (10).

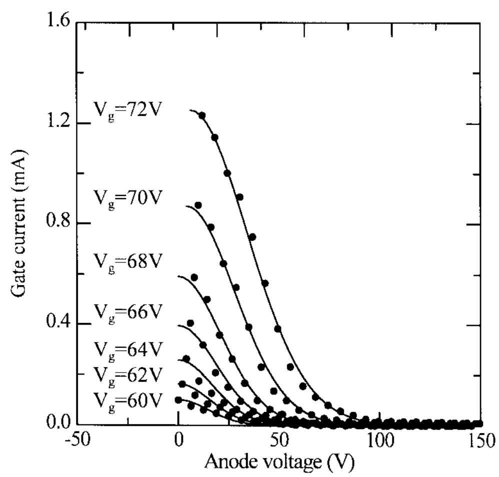

Fig. 12. The reconstructed gate current (the solid curves) and the measured data (the dotted curves) versus V_a.

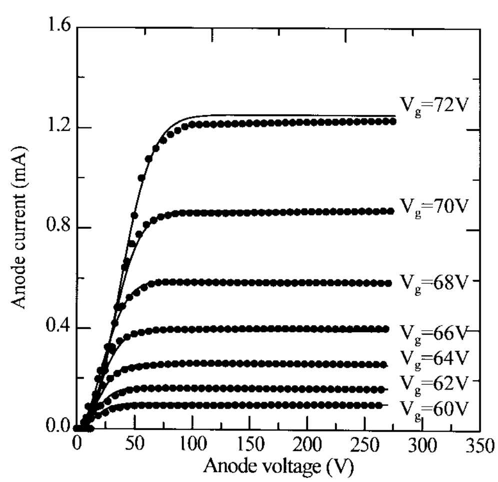

Fig. 13. The reconstructed current data (the solid curves) computed from the extracted values of the model parameters and the original measured data (the dotted curves). Two sets of characteristics match very well.

the data points obtained from [28] and the solid lines are reconstructed curves from the model. The values derived for

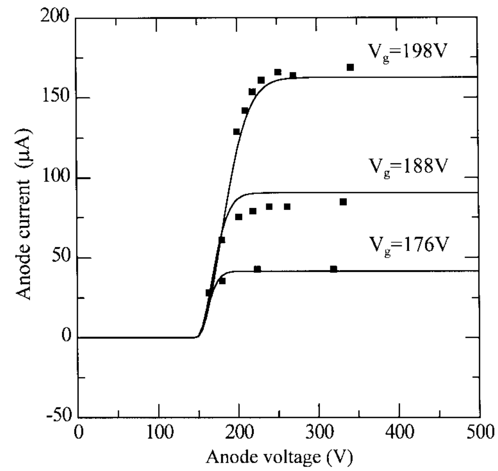

Fig. 14. The *I–V* characteristics of an FET triode with 100 emitter tips. The square curves are the measured data which were obtained from the Holland's paper [28]. The solid lines are the reconstructed curves from the model.

TABLE II
EXTRACTED PARAMETERS OF THE SECOND EXAMPLE

Parameter or Term	Value or Function
A'	$6.78\times10^{-8}\ A/V^3$
B'	$1.6\times10^{3}\ V$
$\frac{2\pi r^2 NA}{\lambda B}\beta^3$	$6.69\times10^{-8}+9.46\times10^{-11}\ V_g$
V_{aT}	147 V
a_0	7.92 degrees/volts
a_1	-3.67×10^{-2} degrees/volts
a_2	0 degrees/volts
r	17.7nm

the parameters are summarized in the Table II. This example also verify the accuracy of the model.

IV. Conclusion

In this work, a simple but accurate physical model for FET device has been developed. The model can be used in the circuit simulation programs such as SPICE. For the model, the cathode current based on the F–N relationship is obtained by integration of current density on the surface of the emission tip. The emission angle θ_e is introduced to describe the emission area. The gate current is derived by same integration but on a different emitting area. A procedure to extract the values for the model parameters has also been given. The model has been applied to experimental FET devices to demonstrate its accuracy.

References

[1] P. Vaudaine and R. Meyer, "Microtips fluorescent display," in *IEEE IEDM*, 1991, pp. 197–200.

[2] D. A. Cathey, Jr., "Field emission display," in *Int. Symp. VLSI Technology, Systems, and Applications. Proc. Technical Papers*, 1995, pp. 131–136.

[3] J. M. Kim, B. I. Gorfinkel, J. H. Kang, E. V. Roussina, J. W. Kim, I. V. Chernyaeva, J. H. Choi, and A. R. Zoukarneev, "4″ field emission display development and its reliability analysis," in *Tech. Dig. IVMC'96*, 1996, pp. 566–570.

[4] L. J. Huangfu, C. C. Zhu, Y. J. Huai, Z. L. Tie, Y. Li, and C. Guo, "Research on the processing of vacuum microelectronic flat-panel displays," in *Tech. Dig. IVMC'96*, 1996, pp. 581–584.

[5] G. Gammie, R. Kozlowski, R. Mallavarpu, and A. Palevsky, "Field emission arrays for microwave applications," in *IEEE IEDM*, 1993, pp. 753–756.

[6] P. M. Phillips, R. E. Neidert, L. Malsawma, and C. Hor, "Microwave triode amplifiers from 1–2 GHz using molybdenum thin-film-field-emission cathode devices," *IEEE Trans. Electron Devices*, vol. 42, pp. 1674–1680, 1995.

[7] C. A. Spindt, C. E. Holland, P. R. Schwoebel, and I. Brodie, "Field-emitter-array development for microwave applications," in *Tech. Dig. IVMC'96*, 1996, pp. 638–639.

[8] R. H. Fowler and L. Nordheim, "Electron emission in intense electric fields," in *Proc. Royal Soc. London*, vol. 119a, pp. 173–181, 1928.

[9] C. A. Spindt, I. Brodie, L. Humphrey, and E. R. Westerberg, "Physical properties of thin-film field emission cathodes with molybdenum cones," *J. Appl. Phys.*, vol. 47, no. 12, Dec. 1976.

[10] W. J. Orvis, C. F. McConaghy, D. R. Ciarlo, J. H. Yee, and E. W. Hee, "Modeling and fabricating micro-cavity integrated vacuum tubes," *IEEE Trans. Electron Devices*, vol. 36, p. 2651, 1989.

[11] K. Betsui, "Fabrication and characteristics of Si field emitter arrays," in *Tech. Dig. IVMC'91*, 1991, pp. 26–29.

[12] H. H. Busta, J. E. Pogemiller, and B. J. Zimmerman, "Collector-assisted operation of micromachined field-emitter triodes," *IEEE Trans. Electron Devices*, vol. 40, pp. 1537–1542, 1993.

[13] C. A. Spindt, I. Brodie, L. Humphrey, and E. R. Westerberg, "Physical properties of thin-film field emission cathodes with molybdenum cones," *J. Appl. Phys.*, vol. 47, pp. 5248–5263, 1976.

[14] W. A. Mackie, C. H. Hinrichs, and P. R. Davis, "Preparation and characterization of zirconium carbide field emitters," *IEEE Trans. Electron Devices*, vol. 36, pp. 2697–2702, 1989.

[15] D. Nicolaescu and V. Avramescu, "Field emission diode characterization through model parameters extraction from current-voltage experimental data," *J. Vac. Sci. Technol. B*, vol. 12, no. 2, pp. 749–754, Mar./Apr. 1994.

[16] D. A. Kirkpatrick, A. Mankofsky, and T. Tsang, "Analysis of field emission from three-dimensional structures," *Appl. Phys. Lett.*, vol. 60, pp. 2065–2067, 1992.

[17] D. Nicolaescu, "Physical basis for applying the Fowler–Nordheim J-E relationship to experimental I-V data," *J. Vac. Sci. Technol. B*, vol. 11, no. 2, pp. 392–395, 1993.

[18] H. H. Busta, B. J. Zimmerman, M. C. Tringides, and C. A. Spindt, "DC I-V characteristics of field emitter triodes," *IEEE Trans. Electron Devices*, vol. 38, pp. 2558–2562, 1991.

[19] R. D. Jones, R. K. Feeney, J. K. Cochran, and D. N. Hill, "A circuit model for a family of low-voltage field-emission-array cathodes," in *Tech. Dig. IVMC'95*, 1995, pp. 72–76.

[20] M. Qin, Q. A. Huang, and T. L. Wei, "A circuit model for a vertical vacuum microelectronic triode at high frequency," in *Tech. Dig IVMC'96*, 1996, pp. 86–90.

[21] C. W. Lu, C. L. Lee, and J.M. Huang, "A SPICE simulation model for field emission triode," in *Tech. Dig. IVMC'96*, 1996, pp. 62–66.

[22] T. Utsumi, "Keynote address vacuum microelectronics: What's new and exciting," *IEEE Trans. Electron Devices*, vol. 38, pp. 2276–2283, 1991.

[23] G. N. A. van Veen, "Space-charge effects in spindt-type field emission cathodes," *J. Vac. Sci. Technol. B*, vol. 12, no. 2, pp. 655–661, Mar./Apr. 1994.

[24] K. L. Jensen, E. G. Zaidman, M. A. Kodis, B. Goplen, and D. N. Smithe, "Analytical and semi-numerical models for gated FEA's," in *Tech. Dig. IVMC'95*, 1995, pp. 216–220.

[25] H. H. Busta, J. E. Pogemiller, and B. J. Zimmerman, "Emission characteristics of silicon vacuum triodes with four different gate geometries," *IEEE Trans. Electron Devices*, vol. 40, pp. 1530–1536, 1993.

[26] P. H. Cutler, J. He, N. M. Miskovski, T. E. Sullivan, and B. Weiss, "Theory of electron emission in high fields from atomically sharp emitters: Validity of the Fowler–Nordheim equation," *J. Vac. Sci. Technol. B*, vol. 11, no. 2, pp. 387–391, 1993.

[27] J. M. Houston, "The slope of logarithmic plots of the Fowler-Nordheim equation," *Phys. Rev.*, vol. 88, no. 2, p. 349, Oct. 15, 1952.

[28] C. E. Holland, A. Rosengreen, and C. A. Spindt, "A study of field emission microtriodes," *IEEE Trans. Electron Devices*, vol. 38, pp. 2368–2372, 1991.

Chi-Wen Lu was born in Tainan, Taiwan, R.O.C., on October 11, 1965. He received the B.S. degree in electronic engineering from National Taiwan Institute of Technology, Taipei, in 1991, and the M.S. degree in electro-optics from National Chiao Tung University, Hsinchu, Taiwan, in 1994, where he is currently pursuing the Ph.D. degree in the Department of Electronics Engineering. His Ph.D research focuses on the modeling of field emitter transistor, the driver circuit design for field emission display, the built-in current sensor design for IDDQ testing and the methodology of IDDQ testing for deep-submicron circuit.

Chung Len Lee (S'70–M'75–SM'92), photograph and biography not available at the time of publication.